

Journal of Materials Chemistry C

Accepted Manuscript



This is an *Accepted Manuscript*, which has been through the Royal Society of Chemistry peer review process and has been accepted for publication.

Accepted Manuscripts are published online shortly after acceptance, before technical editing, formatting and proof reading. Using this free service, authors can make their results available to the community, in citable form, before we publish the edited article. We will replace this *Accepted Manuscript* with the edited and formatted *Advance Article* as soon as it is available.

You can find more information about *Accepted Manuscripts* in the [Information for Authors](#).

Please note that technical editing may introduce minor changes to the text and/or graphics, which may alter content. The journal's standard [Terms & Conditions](#) and the [Ethical guidelines](#) still apply. In no event shall the Royal Society of Chemistry be held responsible for any errors or omissions in this *Accepted Manuscript* or any consequences arising from the use of any information it contains.

Hydrothermal Growth and Optical Properties of Nb₂O₅ Nanorod Arrays

Cite this: DOI: 10.1039/x0xx00000x

Received 00th January 2012,
Accepted 00th January 2012

DOI: 10.1039/x0xx00000x

www.rsc.org/

Jing He^a, Yongming Hu^{a,†}, Zhao Wang^a, Wei Lu^b, Shulin Yang^a, Guitai Wu^a, Yu Wang^b, Shengfu Wang, Haoshuang Gu^{a,†}, John Wang^c

Nb₂O₅ nanorod arrays were grown on Nb foil through an *in-situ* hydrothermal treatment process using NH₄F as the mineralizing agent and H₂O₂ as the oxidant. The as-prepared Nb₂O₅ nanorod arrays were well crystallized with hexagonal structure and *c*-axis orientation. The effects of hydrothermal temperature and concentration of NH₄F on the growth of nanorods were investigated. Nb₂O₅ nanorod arrays are formed by crystal nucleation, oriented growth, and then orientation attachment. A higher concentration of NH₄F accelerates the generation of Nb₂O₅ nanorods as a result of corroding Nb foil and releasing Nb ions, and promotes the oriented growth of Nb₂O₅ nanorods. The band gap of Nb₂O₅ nanorod arrays is measured to be about 3.3 eV, which exhibit a blue light emission located at 456 nm (2.719 eV) and a cyan light emission located at 490 nm (2.53 eV) respectively. The 2.53 eV peak can well be attributed to the donor-acceptor pair (DAP) emission, and the 2.719 eV peak be related to the conduction-band-to-acceptor transitions. There is only one quenching channel for 2.719 eV peak with increasing temperature, which corresponds to the activation energy of about 16.9 meV, according to the theoretical fitting.

Introduction

One-dimensional (1D) nanostructures of semiconductor oxides promise great application potentials in optical, electrical and magnetic micro/nano-scaled devices, such as field emission displays, energy conversion cells, high-density storage memories, microelectronic devices and chemical sensors.¹⁻⁴ Among them, the wide band gap semiconductor oxides, such as ZnO nanowires/nanobelts and TiO₂ nanorods/nanotubes have been extensively investigated owing to their excellent and particular physical and chemical properties.^{5,6} For instance, *c*-axis vertically aligned ZnO nanorod arrays have been synthesized on ZnO thin film via hydrothermal route, which showed a high sensitivity to H₂ at room temperature and a detection limit of 20 ppm.⁷ However, ZnO is deliquescent and liable to degradation due to moisture absorption, which would limit the practical application of ZnO nanomaterials-based nanodevice under harsh environment.

Niobium oxide is another important semiconductor oxide with superior photocatalyst⁸, gas sensing^{9,10}, electrochromic¹¹ and biosensing performances¹². Among the different stoichiometries of niobium oxide, Nb₂O₅ is thermodynamically stable, of chemical inertness and low cytotoxicity. Up to now, a variety of approaches have been employed for the growth of Nb₂O₅ 1-D nanostructures, including thermal oxidation⁹, anodic oxidation¹³, plasma oxidation¹⁴, phase transformation¹⁵ and hydrothermal method¹⁶. Among them, hydrothermal method has been recognized as a simple, inexpensive and low-temperature method for the growth of single-crystalline oxide nanostructures. For example, single crystalline Nb₂O₅ nanorods were developed by hydrothermal process at 200 °C for ~30 days using metal Nb powder and water as the starting materials.¹⁷ Based on this work, orthorhombic phased Nb₂O₅ (O-Nb₂O₅) nanorod array films with [001] orientation were synthesized by the hydrothermal method in ammonium fluoride (NH₄F) aqueous solution environment followed by annealing

treatment at 300-500 °C.¹⁶ However, the crystallinity of the as-prepared hydrothermal samples is poor and needs to be further improved by annealing at relatively higher temperatures, which however can result in the secondary growth of the grains and orientation changes. Moreover, the exact growth mechanism and behavior of Nb₂O₅ nanorods are unclear, which may limit the controllable synthesis of nanorod arrays.

It has been reported that simultaneous addition of hydrogen peroxide (H₂O₂) and NH₄F play a pivotal role in the dissolution of metallic titanium, generating and improving the crystallinity of TiO₂ nanomaterials.¹⁸ In this work, well-crystallized hexagonal Nb₂O₅ (H-Nb₂O₅) nanorod arrays were synthesized on Nb foil by a one-step hydrothermal process. The growth process and mechanism of Nb₂O₅ nanorod arrays are investigated. The temperature dependent photoluminescence (PL) properties and light emission mechanism of Nb₂O₅ nanorod arrays are studied.

Experimental details

With NH₄F as the mineralizing agent and H₂O₂ as the oxidant, Nb₂O₅ nanorod arrays were *in-situ* synthesized on Nb foil by hydrothermal method. Firstly, 0.25 to 1 g of NH₄F was dissolved into a 1:1 mixture of hydrogen peroxide (H₂O₂, 30 wt.%) and deionized (DI) water (20 ml for each) in a Teflon-lined autoclave (50 mL in volume). After stirring, a piece of ultrasonically cleaned Nb foil of 250 μm in thickness was immersed into the above solution. The autoclave was then sealed and positioned into the oven for hydrothermal treatment at 125-175 °C for 5-20 h. After naturally cooling to room temperature, the as-prepared samples were rinsed with DI water for several times and dried at 80°C in air.

The phases in the resultant nanorods were characterized by X-ray diffraction (XRD Bruker D8A25, CuKα, λ = 1.54184 Å). Their morphologies were characterized by field emission scanning electron microscopy (FESEM, JOEL JSM-7100F).

Their microstructure was studied by using transmission electron microscopy (TEM, JEOL Model JEM-2011). The photoluminescence (PL) spectra measurements were performed on Steady-state Spectrofluorometer (JOBIN YVON, type FLUOROLOG-3-TAU) using a Xe lamp (150 W) as the light source. The temperature-dependent PL measurements were conducted at temperatures from 9 to 300 K.

Results and discussion

Hydrothermal growth of Nb₂O₅ nanorod arrays

Hydrothermal temperature is a crucial factor for the growth of oxide nanostructures. **Fig. 1(a-c)** shows the XRD patterns of the as-prepared samples synthesized by the hydrothermal process at different hydrothermal temperatures for 15 h using 12.5 M NH₄F and 20 ml H₂O₂ as the mineralizing agent and oxidant respectively. Sharp diffraction peaks indicate the samples are well crystallized after the *in-situ* hydrothermal treatment. The characteristic diffraction peaks of (001), (100), (101), (002) and (102) are indexed into hexagonal phase (H-Nb₂O₅) according to JCPDS Card No. 28-0317. The other diffraction peaks at around 38.5° (110) and 55.3° (200) belong to the cubic metal Nb. The samples are therefore of highly *c*-axis orientation according to the intense (001) diffraction peaks, and the intensity become stronger with increasing hydrothermal temperature, which could well be attributed to the higher growth rate of Nb₂O₅ at higher temperature. The diffraction peaks of (001) and (002) of the as-prepared samples minor were noted to shift to high-angle, and (100), (101) shift to low-angle a little compared to the standard card¹⁹. An inner stress is expected to occur when the metal Nb is transferred into Nb₂O₅ *in-situ* due to the rather different lattice parameters.

(Fig.1)

Fig. 1 The XRD patterns of the as-prepared Nb₂O₅ nanorod arrays synthesized by hydrothermal method at different temperatures using 12.5M NH₄F and 20ml H₂O₂ (30 wt.%). (a) 125 °C; (b) 150 °C; (c) 175 °C.

(Fig.2)

Fig. 2 SEM images of the as-prepared Nb₂O₅ nanorod arrays synthesized by hydrothermal method at different temperatures using 12.5M NH₄F and 20ml H₂O₂ (30 wt.%). (a) 125 °C; (b) 150 °C; (c) 175 °C.

Fig. 2 shows the SEM images of the as-synthesized Nb₂O₅ samples, where one can see that Nb₂O₅ nanorods with uniform diameters were developed by hydrothermal process at temperatures from 125 to 175 °C. According to top view and cross-section view of SEM images, the sample obtained at 125 °C was consisting of short hexagonal-type nanorods with ~ 400 nm in diameter, and the rod number density of nanorods as high as 5.3×10^9 rods/cm² (~ 850 nm in length). With the increase in reaction temperature to 150 °C, the aspect ratio of Nb₂O₅ nanorods and the spacing between nanorods were obviously increased, and the observed rod number density decreases to about 4.5×10^9 rods/cm². For the sample obtained at 175 °C,

the aspect ratio and spacing of Nb₂O₅ nanorods were increased further, the typical diameter and the rod number density were of 430 nm and 3.94×10^9 rods/cm², respectively, which indicate that a higher hydrothermal temperature reduces the nucleation rate and promotes the oriented growth of Nb₂O₅ nanorods. For comparison purpose, **Fig.1S** shows the XRD pattern and SEM image of the sample annealed in O₂ atmosphere at 500°C for 1h. One can see that the annealed sample is of an orthorhombic phase according to JCPDS Card No. 27-1003, which is corresponding to the result reported by Wen *et al*¹⁶. In addition, the morphology of individual nanorod is almost unchanged except for the nanoarrays crack due to the release of lattice stress.

The mineralizer concentration in hydrothermal chamber was another predominant factor that influences the crystallinity and morphology of the nanorod products. The XRD patterns of the as-synthesized samples using 20 ml H₂O₂ (30 wt.%) and at various NH₄F concentrations at 150 °C for 15 h were shown in **Fig. 3**. One can see that the intermediated products contain Nb, O and F atoms (according to the EDS results shown in **Fig. 2S**) and no H-Nb₂O₅ phase were obtained using 20 ml H₂O₂ and 5.00 M of NH₄F as the oxidant and mineralizer, respectively, as shown from the peaks denoted by “star” symbols in Fig.3a. With the NH₄F concentration being increased to 8.75 M, the diffraction peaks belong to the H-Nb₂O₅ gradually appeared, and the intermediated products gradually disappeared (Fig.3b). The single phased H-Nb₂O₅ is formed when the concentration of NH₄F is reaching to 12.5 M. The relative amount of Nb₂O₅ against Nb foils therefore increases with the increasing NH₄F concentrations further (Fig.3c-3e), indicated by the variation of relative diffraction intensity, which could be attributed to the higher growth rate of Nb₂O₅ at higher concentrations of NH₄F.

(Fig.3)

Fig. 3 XRD patterns of the as-synthesized samples using 20ml H₂O₂ (30 wt.%) and different NH₄F concentrations: (a) 5.00 M; (b) 8.75 M; (c) 12.50 M; (d) 18.75 M; (e) 25.00 M

Fig. 4 shows the corresponding SEM images of the as-synthesized samples using 20 ml H₂O₂ (30 wt.%) and various NH₄F concentrations. As shown in Fig.4a, H-Nb₂O₅ nanorod arrays with uniform diameters of about 550 nm, the rod number density of about 2.5×10^9 rods/cm² and hexagonal shaped cross-section can be obtained as NH₄F concentration being increased to 8.75 M. It seems like that the diameters became larger and the hexagonal shape nanorod transformed into rounded shape when the concentration of NH₄F is increased from 8.75 to 25 M. One can consider that each rod is composed of several rods with smaller diameters under higher concentration of NH₄F, as shown from the cross-section view in the inset of Fig.4b. The exact rod number density could not be offered here due to the faint nanorods boundaries. It can be concluded that a higher concentration of NH₄F would result in an increase in supersaturation and thus higher nucleation rate, which promotes the radial growth of nanorods and formation of micrometer rods Nb₂O₅. In addition, the emergence of new

nucleation sites on the surface of Nb₂O₅ rods as shown by white arrow in **Fig. 4c**.

(Fig.4)

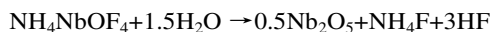
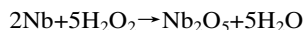
Fig. 4 SEM images of the as-synthesized samples using 20 ml H₂O₂ (30 wt.%) and different NH₄F concentrations at 150 °C for 15 h: (a) 8.75 M; (b) 18.75 M; (c) 25M

For TEM characterization, Nb₂O₅ nanorods grown at 150 °C for 15 h using 20 ml H₂O₂ (30 wt.%) and 12.5 M NH₄F were chosen. The sharp diffraction spots in SAED pattern shown in the inset in **Fig. 5a** demonstrate that each of the Nb₂O₅ nanorods is single crystalline. The lattice fringe parallel to the end face of the nanorod is clearly recognized in the high-resolution TEM (HRTEM) image shown in **Fig. 5b**. The fringe spacing is calculated to be ~ 0.39 nm corresponding to the (001) lattice spacing, which indicated [001] is the preferred growth direction of the as-synthesized Nb₂O₅ nanorods.

(Fig.5)

Fig. 5 The TEM images of a single Nb₂O₅ nanorod prepared with 20 ml H₂O₂ (30 wt.%) and 12.5 M NH₄F at 150 °C for 15 h: (a) TEM image and SAED patterns (inset); (b) HRTEM image.

In order to understand the growth behavior of Nb₂O₅ nanorods under the hydrothermal conditions, a series of Nb₂O₅ samples were synthesized by hydrothermal process using 20 ml H₂O₂ (30 wt.%) and 12.5 M NH₄F at 150 °C with reaction time being varied from 5 to 20 h. The XRD patterns shown in **Fig. 3S** confirmed that all samples are H-phase of Nb₂O₅. The variation in length and aspect ratio of the nanorods were shown in **Fig. 6**. There is a steady increase in the lengths of nanorods, while the aspect ratio of nanorods shows a first increase and then a reduction with increasing hydrothermal time. As previously reported in the literature¹⁶, Nb₂O₅ nanostructures were formed according to the following chemical process: F⁻ was used to attack Nb metal or niobium oxide precursor to form fluoride containing intermediate compounds (NH₄)₂NbOF₅, then transferred into more stable NH₄NbOF₄ by releasing one NH₄F molecule under hydrothermal condition. Nb₂O₅ is then obtained after the decomposition of NH₄NbOF₄. In this work, NH₄F and H₂O₂ were used as the mineralizing agent and oxidant together in the hydrothermal environmental, the following chemical reactions are expected to occur in the hydrothermal process:



At the beginning of the hydrothermal reaction, Nb foil was etched by NH₄F directly to release Nb ions and is oxidized by H₂O₂ indirectly. It's noted that the by-products of NH₃ and HF

might react and transfer into NH₄F again and to conserve the amount of mineralizer. As shown in **Fig. 6a**, the sample consisted of a large amount of aggregated nanoparticles (buffer layer) after the hydrothermal treatment for 5 h, which is considered as the nucleation stage for the growth of Nb₂O₅ nanorods. During the hydrothermal process, there would be a compressive stress generated at the interface between Nb₂O₅ and Nb foil due to the different lattice parameters²⁰, which makes Nb₂O₅ nucleus grew quickly. The oriented growth of Nb₂O₅ became the major process upon the formation of the buffer layer, and resulted in an increase of aspect ratio of nanorods (a→b).²¹ As the hydrothermal time exceeded to 10 hours (**Fig. 6c**), nanorods became dense and limited the release of Nb atoms into the solution. Then the nanorods tend to growth together due to the interfacial lattice matching between Nb₂O₅ nanorods through orientation attachment.

(Fig.6)

Fig. 6 The relationships between the average length and aspect ratio of the as-synthesized Nb₂O₅ nanorods as a function of hydrothermal time. The scale bar in the inset SEM images is 5 μm in length: (a) 5 h; (b) 10 h; (c) 15 h; (d) 20 h.

Photoluminescence properties of Nb₂O₅ nanorod arrays

The room temperature excitation spectrum and temperature dependent emission spectra of the Nb₂O₅ nanorod arrays are shown in **Fig. 7**. The Nb₂O₅ nanorod arrays demonstrate the strongest excitation peak at 379 nm, indicating the band gap is about 3.3 eV, which is consistent with the reported values of Nb₂O₅ synthesized with different methods (3.2 - 4.8 eV).²²⁻²⁴ There are two light emission peaks at low temperature (9 K) located at 456 nm (2.719 eV) and 490 nm (2.53 eV) respectively, which are due to fluorescence quenching occurred easily²⁵. One can see that the intensity of the 2.719 eV peak becomes dominant with increasing temperature from 9 to 300 K, while the 2.53eV peak diminishes gradually (from 9 to 140 K) and its peak position blue-shifts slightly (about 166 meV) which are the typical features of donor-acceptor pair (DAP) emission²⁶. Therefore, the 2.53 eV peak is attributed to the DAP emission, and the 2.719 eV peak is related to the conduction-band-to-acceptor transitions.

(Fig.7)

Fig. 7 (a) The room temperature excitation spectrum and temperature dependent emission spectrum (λ_{ex} = 379 nm) of the Nb₂O₅ nanorod arrays, which are obtained by hydrothermal method using 12.5 M NH₄F and 20 ml H₂O₂ (30 wt.%) as the mineralizing agent and oxidant at 150 °C for 15h.

(Fig.8)

Fig. 8 The integrated PL intensities of the 2.719 eV peak as a function of reciprocal temperature, in which the scattered squares are experimental data, the dot curve is the theoretical fitting result.

In order to determine the thermal quenching of 2.719 eV emissions, activation energy needs to be introduced to describe the PL quenching process. The variation in PL intensity of the conduction-band-to-acceptor transition with reciprocal temperature is shown in **Fig. 8**. The curve represented by the squares is the experimental data, which can be well described by the theoretical fit of the following expression²⁷:

$$I = I_0 / [1 + a_1 \exp(-E_{a1} / kT) + a_2 \exp(-E_{a2} / kT)]$$

where $I(T)$ and I_0 are the PL intensities at temperature T and 0K, respectively. a_1 and a_2 are constants, E_{a1} and E_{a2} are activation energy for thermal quenching, and k is the Boltzmann constant. Considering that there is only a single channel contributing to the thermal quenching of the 2.719 eV peak emission by making a_2 zero in the above equation, one can obtain the best fitting result in **Fig. 8**, which indicate that there is only one quenching channel for 2.719 eV peak. The curve fit gives rise to activation energy of about 16.9 meV. The E_a value obtained here is almost identical to that reported by Wen et al. in ZnO/ZnMgO multiple quantum wells,²⁸ which indicating Nb₂O₅ nanorod arrays have great prospects in optoelectronics applications in the wavelength range from the ultraviolet to the red.

Conclusions

C-axis oriented Nb₂O₅ nanorod arrays with H-phase structure were synthesized by in-situ hydrothermal process using NH₄F and H₂O₂ as the mineralizing agent and oxidant, respectively. NH₄F promotes the crystallization and oriented growth of Nb₂O₅ nanorods by increasing the oriented growth rate. Lower temperature/higher concentration of NH₄F could result in an increase in supersaturation and thus higher rod number densities. The growth processes of Nb₂O₅ nanorod arrays include crystal nucleation, oriented growth, and orientation attachment. The Nb₂O₅ nanorod arrays exhibit an excitation peak at 379 nm, indicating that the band gap is about 3.3 eV. There are two obvious emission peaks located at 456 nm (2.719 eV) and 490 nm (2.53 eV) at low temperature, which is shown to derive from the conduction-band-to-acceptor transition and donor-acceptor air emission. There is only one quenching channel for 2.719 eV peak with activation energy of about 16.9 meV. Nb₂O₅ nanorod arrays have potential application in nano-scaled sensor and optoelectronic device etc.

Acknowledgements

This work was financially supported by the National Science Foundation of China (Grand No. 61274073), the National High Technology Research and Development Program of China (Grand No. 2013AA031903), the Applied Basic Research Programs of Wuhan city (Grand No. 2014010101010006), the Outstanding Young Academic Backbone Talents of Hubei Province of China, and the Key Project of Natural Science Foundation of Hubei Province of China (Grand No. 2013CFA043).

Notes and references

^a Hubei Collaborative Innovation Center for Advanced Organic Chemical Materials, Faculty of Physics & Electronic Science, Hubei University, Wuhan 430062, P R China

^b Department of Applied Physics and Materials Research Centre, The Hong Kong Polytechnic University, Kowloon, Hong Kong SAR, PR China.

^c Department of Materials Science & Engineering, Faculty of Engineering, National University of Singapore, BLK E3A, #04-10, 7 Engineering Drive 1, Singapore

† Corresponding Authors, E-mail: yongming.hu09@gmail.com, guhsh583@hubu.edu.cn.

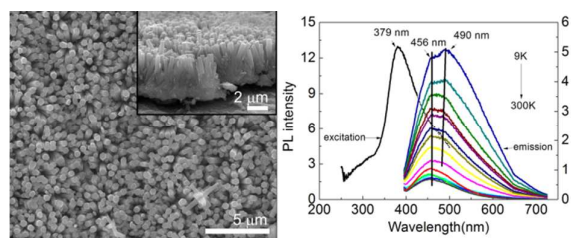
Electronic Supplementary Information (ESI) available: [details of any supplementary information available should be included here]. See DOI: 10.1039/b000000x/

- H. Zeng, X. Xu, Y. Bando, U. K. Gautam, T. Zhai, X. Fang, B. Liu and D. Golberg, *Adv Funct Mater*, 2009, **19**, 3165-3172.
- Z. Wen, L. Zhu, W. Mei, L. Hu, Y. Li, L. Sun, H. Cai and Z. Ye, *Sensor Actuat B-chem*, 2013, **186**, 172-179..
- C. An, K. Tang, X. Liu, F. Li, G. Zhou and Y. Qian, *J Cryst Growth*, 2003, **252**, 575-580.
- M.-H. Lee, J. L. Thomas, Y.-L. Chen, C.-F. Lin, H.-H. Tsai, Y.-Z. Juang, B.-D. Liu and H.-Y. Lin, *Biosens Bioelectron*, 2013, **47**, 56-61.
- K. V. Gurav, M. G. Gang, S. W. Shin, U. M. Patil, P. R. Deshmukh, G. L. Agawane, M. P. Suryawanshi, S. M. Pawar, P. S. Patil, C. D. Lokhande and J. H. Kim, *Sensor Actuat B-chem*, 2014, **190**, 439-445.
- H. Zeng, G. Duan, Y. Li, S. Yang, X. Xu and W. Cai, *Adv Funct Mater*, 2010, **20**, 561-572.
- J. X. Wang, X. W. Sun, Y. Yang, H. Huang, Y. C. Lee, O. K. Tan and L. Vayssieres, *Nanotechnology*, 2006, **17**, 4995-4998.
- S. S. Arbuj, R. R. Hawaldar, U. P. Mulik and D. P. Amalnerkar, *Journal of Nanoengineering and Nanomanufacturing*, 2013, **3**, 79-83.
- Z. Wang, Y. Hu, W. Wang, X. Zhang, B. Wang, H. Tian, Y. Wang, J. Guan and H. Gu, *Int J Hydrogen Energ*, 2012, **37**, 4526-4532.
- R. A. Rani, A. S. Zoolfakar, J. Z. Ou, M. R. Field, M. Austin and K. Kalantar-zadeh, *Sensor Actuat B-chem*, 2013, **176**, 149-156.
- M. Schmitt, S. Heusing, M. A. Aegerter, A. Pawlicka and C. Avellaneda, *Sol Energ Mater Sol C*, 1998, **54**, 9-17.
- S.-R. Yu, X.-P. Zhang, Z.-M. He, Y.-H. Liu and Z.-H. Liu, *J Mater Sci*, 2004, **15**, 687-691.
- T. Hyodo, J. Ohoka, Y. Shimizu and M. Egashira, *Sensor Actuat B-chem*, 2006, **117**, 359-366.
- U. Cvelbar and M. Mozetič, *J Phys D Appl Phys*, 2007, **40**, 2300.
- C. Yan and D. Xue, *Adv Mater*, 2008, **20**, 1055-1058.
- H. Wen, Z. Liu, J. Wang, Q. Yang, Y. Li and J. Yu, *Appl Surf Sci*, 2011, **257**, 10084-10088.
- H. Luo, M. Wei and K. Wei, *Journal of Nanomaterials*, 2009, **2009**, 1-4.
- L. Lei, C. Yuming, L. Bo, Z. Xingfu and D. Weiping, *Appl Surf Sci*, 2010, **256**, 2596-2601.
- S. Qi, R. Zuo, Y. Liu and Y. Wang, *Mater Res Bull*, 2013, **48**, 1213-1217.
- J. T. Chen, F. Zhang, J. Wang, G. A. Zhang, B. B. Miao, X. Y. Fan, D. Yan and P. X. Yan, *J Alloy Compd*, 2008, **454**, 268-273.

Journal Name

21. M. Guo, P. Diao and S. Cai, *J Solid State Chem*, 2005, **178**, 1864-1873.
22. K. Yoshimura, T. Miki, S. Iwama and S. Tanemura, *Thin Solid Films*, 1996, **281–282**, 235-238.
23. N. Özer, D.-G. Chen and C. M. Lampert, *Thin Solid Films*, 1996, **277**, 162-168.
24. G. Agarwal and G. B. Reddy, *J Mater Sci: Mater Electron*, 2005, **16**, 21-24.
25. X. Y. Zhang, J. Y. Dai, H. C. Ong, N. Wang, H. L. W. Chan and C. L. Choy, *Chem Phys Lett*, 2004, **393**, 17-21.
26. B. P. Zhang, N. T. Binh, Y. Segawa, K. Wakatsuki and N. Usami, *Appl Phys Lett*, 2003, **83**, 1635.
27. H. P. He, H. P. Tang, Z. Z. Ye, L. P. Zhu, B. H. Zhao, L. Wang and X. H. Li, *Appl Phys Lett*, 2007, **90**, 023104.
28. X. Wen, J. A. Davis, L. Van Dao, P. Hannaford, V. A. Coleman, H. H. Tan, C. Jagadish, K. Koike, S. Sasa, M. Inoue and M. Yano, *Appl Phys Lett*, 2007, **90**, 221914.

A table of contents entry



H-Nb₂O₅ nanorod arrays with c-axis orientation were *in-situ* synthesized by hydrothermal process, which exhibit a blue and cyan light emission.

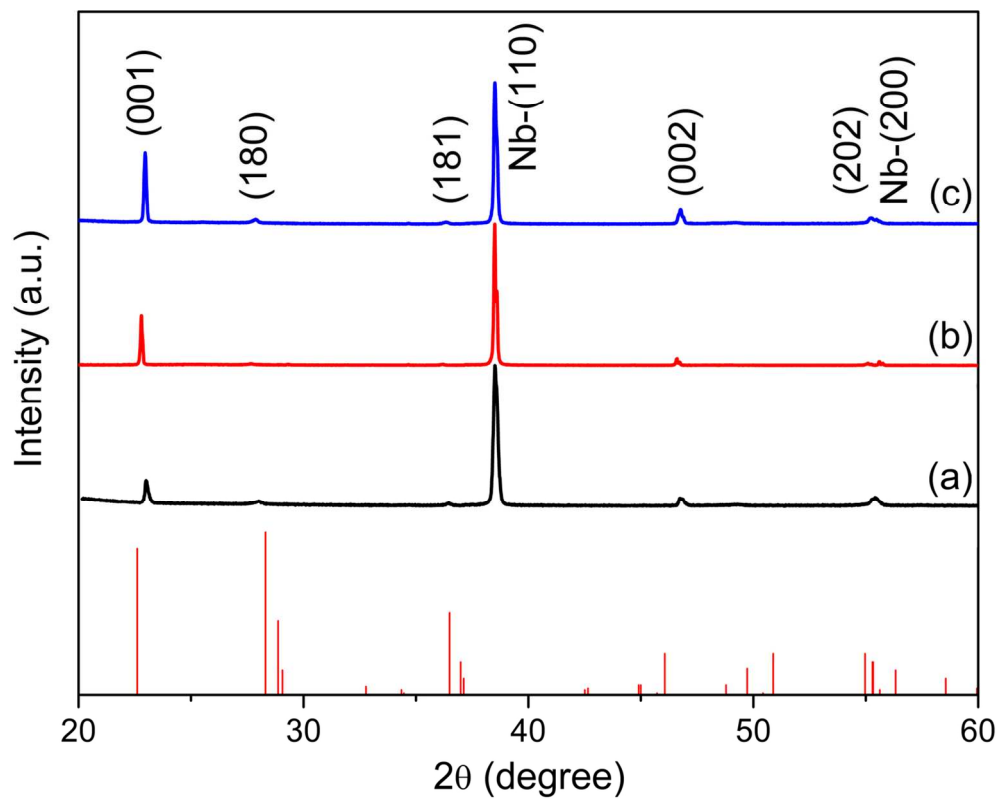


Fig. 1 The XRD patterns of the as-prepared Nb₂O₅ nanorod arrays synthesized by hydrothermal method at different temperatures using 12.5M NH₄F and 20ml H₂O₂ (30 wt.%). (a) 125 °C; (b) 150 °C; (c) 175 °C.
63x50mm (600 x 600 DPI)

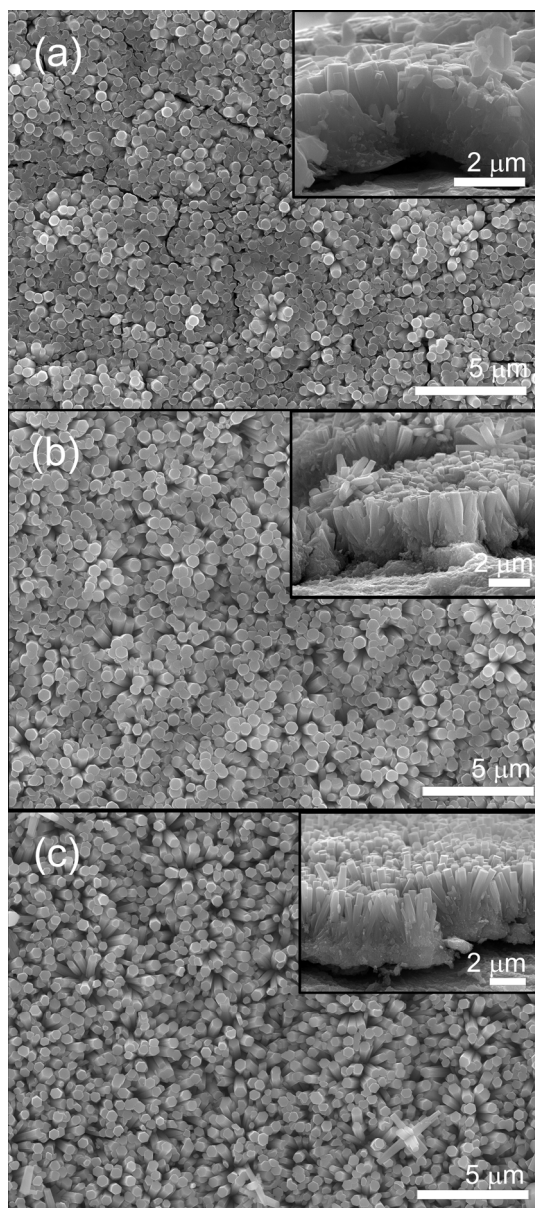


Fig. 2 SEM images of the as-prepared Nb₂O₅ nanorod arrays synthesized by hydrothermal method at different temperatures using 12.5M NH₄F and 20ml H₂O₂ (30 wt.%). (a) 125 °C; (b) 150 °C; (c) 175 °C. 135x304mm (300 x 300 DPI)

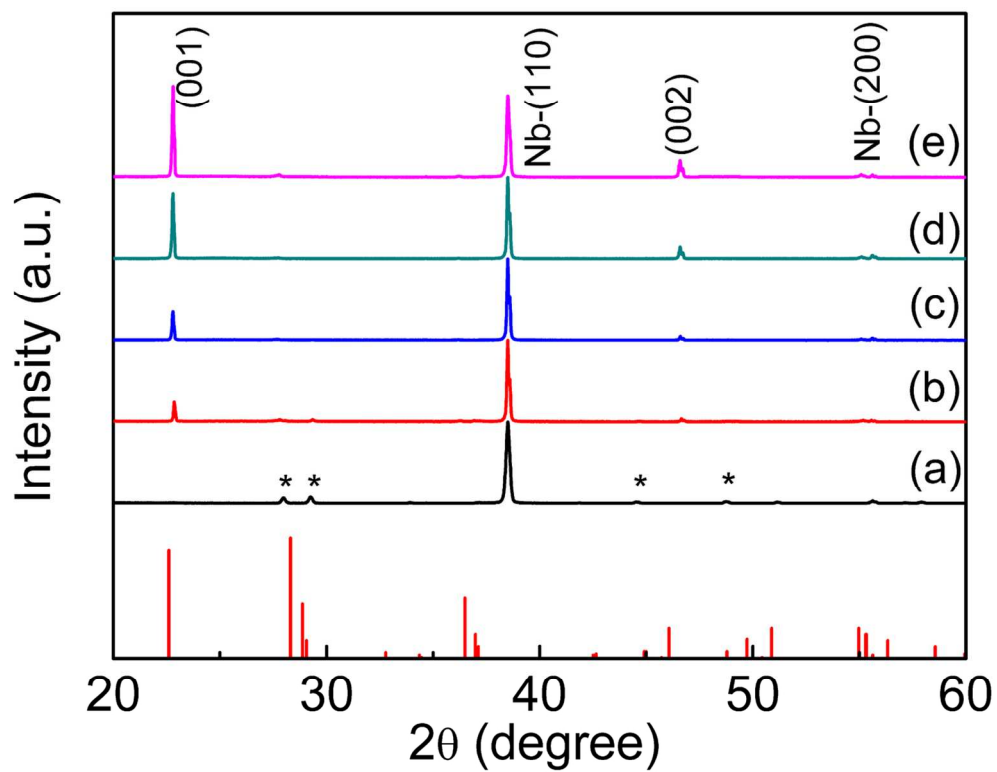


Fig. 3 XRD patterns of the as-synthesized samples using 20ml H₂O₂ (30 wt.%) and different NH₄F concentrations: (a) 5.00 M; (b) 8.75 M; (c) 12.50 M; (d) 18.75 M; (e) 25.00 M
61x46mm (600 x 600 DPI)

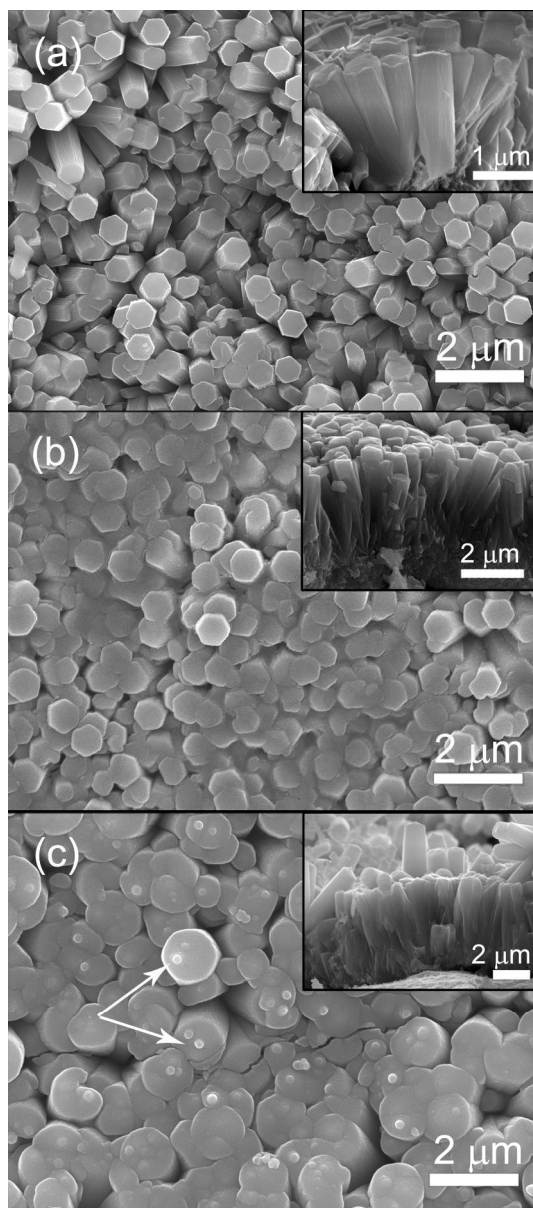


Fig. 4 SEM images of the as-synthesized samples using 20 ml H₂O₂ (30 wt.%) and different NH₄F concentrations at 150 °C for 15 h: (a) 8.75 M; (b) 18.75 M; (c) 25M
135x305mm (300 x 300 DPI)

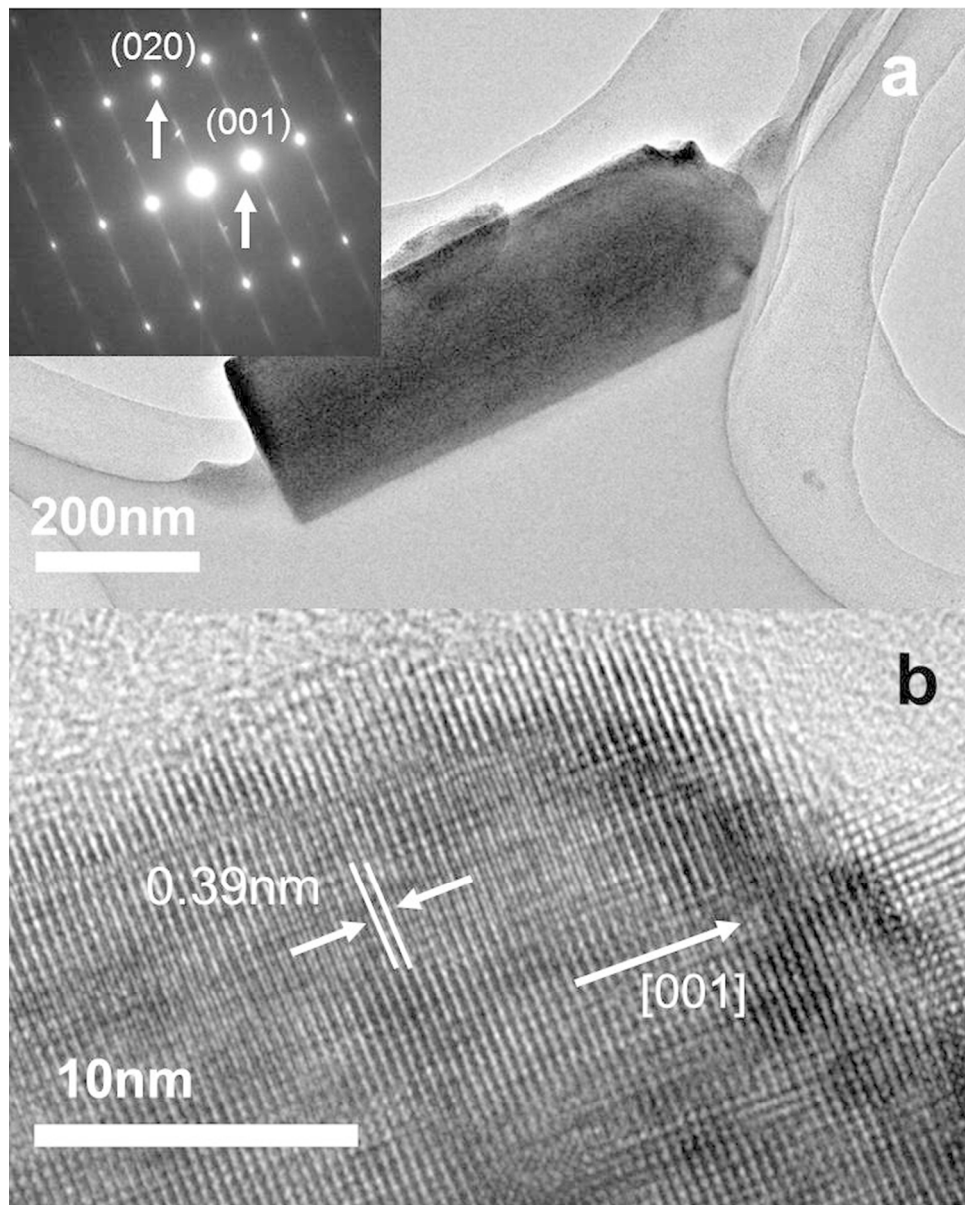


Fig. 5 The TEM images of a single Nb₂O₅ nanorod prepared with 20 ml H₂O₂ (30 wt.%) and 12.5 M NH₄F at 150 °C for 15 h: (a) TEM image and SAED patterns (inset); (b) HRTEM image.
103x128mm (300 x 300 DPI)

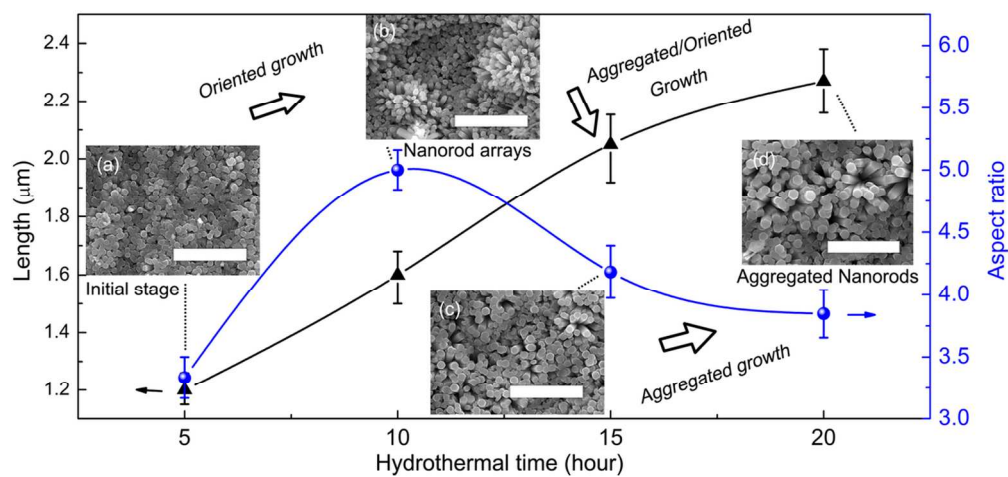


Fig. 6 The relationships between the average length and aspect ratio of the as-synthesized Nb_2O_5 nanorods as a function of hydrothermal time. The scale bar in the inset SEM images is $5 \mu\text{m}$ in length: (a) 5 h; (b) 10 h; (c) 15 h; (d) 20 h.
55x25mm (600 x 600 DPI)

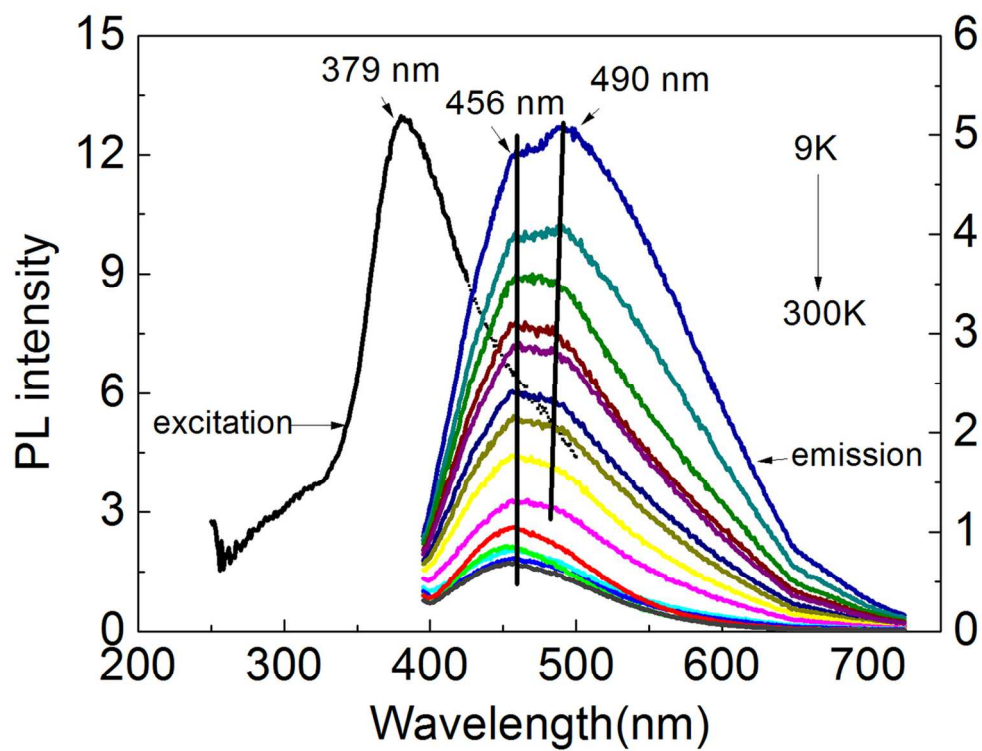


Fig. 7 (a) The room temperature excitation spectrum and temperature dependent emission spectrum ($\lambda_{\text{ex}} = 379 \text{ nm}$) of the Nb₂O₅ nanorod arrays, which are obtained by hydrothermal method using 12.5 M NH₄F and 20 ml H₂O₂ (30 wt.%) as the mineralizing agent and oxidant at 150 °C for 15h.
64x49mm (600 x 600 DPI)

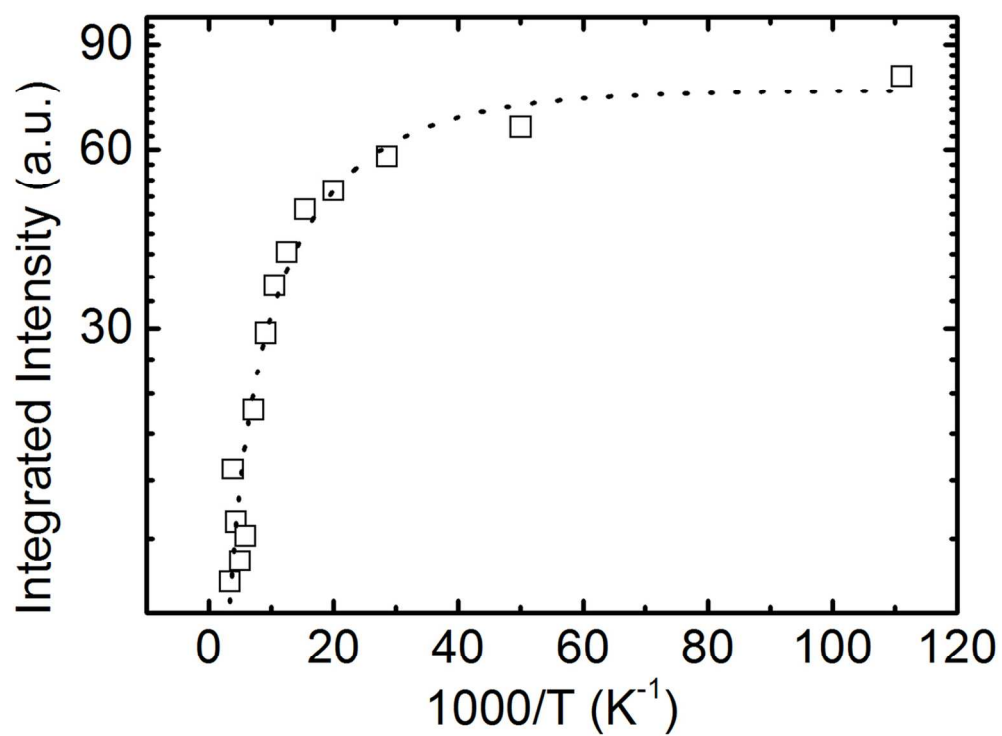


Fig. 8 The integrated PL intensities of the 2.719 eV peak as a function of reciprocal temperature, in which the scattered squares are experimental data, the dot curve is the theoretical fitting result.
62x47mm (600 x 600 DPI)